Comput Mech (2008) 42:593–606
DOI 10.1007/s00466-008-0275-1

ORIGINAL PAPER

A multilevel component mode synthesis approach for the calculation of the phonon density of states of nanocomposite structures

G. Li

Received: 17 July 2007 / Accepted: 8 March 2008 / Published online: 2 April 2008

Abstract In this paper, a multilevel component mode synthesis (MCMS) approach is presented for the calculation of the phonon density of states (PDOS) of nanocomposite structures. In this approach, the nanocomposite structures are described by hierarchical levels of substructures. The phonon frequencies and modes are first computed for the bottom level substructures by using the theory of lattice dynamics. The computed component modes are then synthesized by using a quasi-static component mode synthesis (QSM) technique to obtain the phonon modes of the upper-level substructures in a bottom-up manner. By repeating this procedure, the PDOS of the entire nanostructure can be obtained. The proposed approach, while retains the atomic description of the nanocomposite structure, significantly reduces the computational cost of the calculation. Numerical calculations show that the proposed approach provides accurate results with a much less computational cost. The PDOS of several 1-D atom chains and 2-D atom sheets are computed by using the MCMS.

Keywords Multilevel component mode synthesis · Nanocomposites · Phonon density of states

1 Introduction

Nanocomposites are hybrid materials that combine two or more material components in the nanoscale. Recent research results have shown that nanocomposite materials can have superior mechanical, thermal and electrical properties [1]. Many nanocomposite materials and structures have found applications in nanoelectromechanical systems (NEMS) [2], thermoelectric devices [3–5], engineered bio systems [6] and nanoelectronic circuits [7]. Accurate and efficient calculation of the material properties of nanocomposite materials can accelerate the design and analysis of nanocomposites in various applications as well as deepen the understanding of the material behavior. In determining the mechanical, thermodynamic and electric properties of materials and structures the phonon density of states (PDOS) plays an important role. Specifically, material constitutive relations can be determined by the Helmholtz free energy which is a function of the PDOS [8]. The PDOS is essential in the calculation of thermodynamic properties of materials such as thermal expansion coefficient, heat capacity and thermal conductivity [9–11]. The phonon-limited electrical conductivity in metals is also closely related to the PDOS [12]. Accurate and efficient calculation of the PDOS can help the understanding of the behavior of nanocomposites and the design of novel nanocomposite materials and structures. However, calculating the PDOS of nanocomposite structures can be challenging. Typically, the PDOS can be computed by using the theory of lattice dynamics. Classical approximations of the PDOS, such as the Debye-Einstein approximation [13], only provide coarse descriptions of the phonon spectra. K-space methods [8,9,14] may not be directly applicable for nanocomposites because the periodicity of the crystal structure is lost in nanocomposite structures due to their small size and non-uniform distribution of nanoparticles. Direct calculation of the PDOS in the real space [15] for a nanocomposite structure could become computationally expensive when the structure contains a large number of atoms.

In this work, we seek to accelerate the calculation of the PDOS for nanocomposite structures by employing model order reduction methods. Among various model order

G. Li (✉)
Department of Mechanical Engineering,
Clemson University, Clemson, SC 29631, USA
e-mail: gli@clemson.edu
URL: http://www.ces.clemson.edu/~gli

reduction methods (see [16] for a review), the component mode synthesis method (CMS) [17–21] is a powerful technique for computing the eigen frequencies and eigen modes of large systems. In the CMS, a large structure is discretized into substructures or components. The component modes are computed for each substructure. Only a small set of component modes are retained to construct a set of Ritz basis vectors. The basis vectors are used to approximate the displacements of the substructure. The approximations of the substructures are then assembled to obtain a global approximation of the entire system. While the CMS largely reduces the computational cost for large system analysis, there are drawbacks in the method. First, the degrees of freedom (DOFs) of the substructures can still be large. It can still be expensive to compute the component modes for the substructures. Second, when there are many substructures, the DOFs that are shared by the substructures can become very large. Since the shared DOFs of the substructures are directly included in the reduced-order global system, the size of the global system can also be large. Third, the classical CMS with static constraint mode can be inaccurate in computing intermediate and high frequencies [19,20]. To overcome these difficulties, in this paper, a multilevel component mode synthesis approach (MCMS) is proposed for the calculation of the PDOS of nanocomposite structures. This approach combines a multilevel description of the nanocomposite structure and a quasi-static component mode synthesis method (QSM) [19,20] to efficiently compute the PDOS. The first step of this approach is the hierarchical discretization of the nanostructure. The nanostructure is discretized into substructures or components. Each substructure is then further divided into smaller substructures. The discretization continues to the level where each of the final substructures contains a small number of atoms. From this top-down discretization, the nanostructure is represented by hierarchical levels of substructures. The next step of the approach is constructing the phonon models of the nanostructure in a bottom-up fashion. For the bottom-level substructures, the phonon modes are computed by using the lattice dynamics theory. Since the bottom-level substructures contain only a small number of atoms, the component frequencies and modes can be obtained efficiently. The calculated component modes are then used to obtain the reduced-order systems of the upper-level substructures. In constructing the reduced-order systems, quasi-static constraint modes are computed as described in the QSM [19,20]. The QSM improves the classical CMS to compute the intermediate and high frequencies accurately. By solving the reduced-order systems, the component modes of the upper-level substructures are recovered. This bottom-up procedure continues until the top-level substructure, i.e., the nanostructure itself, is reached. The phonon spectrum of the entire nanostructure can then be obtained. In this paper, the MCMS is applied to compute the PDOS of several 1-D atom chains and 2-D atom sheets. It is shown that the MCMS overcomes the difficulties encountered in the classical CMS, retains the atomic description of the nanostructure, and significantly reduces the computational cost.

The rest of the paper is organized as follows. Section 2 presents the theory of the MCMS, numerical examples are presented in Sects. 3, and 4 presents the conclusions.

2 Theory

2.1 Lattice dynamics

In the theory of lattice dynamics [14], interatomic potentials are employed to describe the interactions between the atoms. Many interatomic potentials have been developed for different materials. For example, Lennard-Jones potential [22] and Morse potential [23] are among the two-body interatomic potentials. Popular many-body potentials include Tersoff [24], Brenner [25] and Stillinger-Weber [26] potentials. For composite materials, multiple interatomic potentials may be necessary in order to describe the interactions between the different kinds of atoms in the system [27–29]. In general. the total potential energy of a system of N atoms can be written as

$$U(\{\mathbf{x}\}) = \frac{1}{2}\sum_{\alpha\neq\beta} V_{\alpha\beta} \qquad \alpha,\beta = 1,2,\ldots,N \tag{1}$$

where $\{\mathbf{x}\} = \{\mathbf{x}_1,\ldots,\mathbf{x}_N\}^T$ is the position vector of the N atoms, $V_{\alpha\beta}$ is the interatomic potential energy between the atoms α and β, and N is the number of atoms in the system. When the system is in thermodynamic equilibrium, the atoms of the system vibrate around their static equilibrium positions. By using the harmonic approximation, the total potential energy of an N-atom system can be written in a quadratic form by neglecting the higher-order (>2) terms in its Taylor's series expansion, i.e.,

$$\begin{aligned} U(\{\mathbf{x}\}) = {} & U\left(\left\{\mathbf{x}^0\right\}\right) \\ & + \frac{1}{2}\sum_{\alpha,\beta=1}^{N}\sum_{i,j=1}^{3} \left.\frac{\partial^2 U(\{\mathbf{x}\})}{\partial \mathbf{u}_{\alpha i}\,\partial \mathbf{u}_{\beta j}}\right|_{\mathbf{x}_1,\ldots,\mathbf{x}_N=\mathbf{x}_1^0,\ldots,\mathbf{x}_N^0} \\ & \times \mathbf{u}_{\alpha i}\mathbf{u}_{\beta j} \qquad i,j = 1,2,3 \end{aligned} \tag{2}$$

where $\left\{\mathbf{x}^0\right\} = \left\{\mathbf{x}_1^0,\ldots,\mathbf{x}_N^0\right\}^T$, $\mathbf{u}_{\alpha i}$ and $\mathbf{u}_{\beta j}$ are the i-th and j-th components of the thermal vibrational displacement of the atoms α and β, respectively. Equation (2) can be rewritten in a matrix form as

$$U(\{\mathbf{x}\}) = U\left(\left\{\mathbf{x}^0\right\}\right) + \frac{1}{2}\{\mathbf{u}\}^T[\mathbf{\Phi}]\{\mathbf{u}\} \tag{3}$$

where $\{\mathbf{u}\} = \{\mathbf{u}_1,\ldots,\mathbf{u}_N\}^T$, and $[\mathbf{\Phi}]$ is the $3N \times 3N$ force constant matrix given by

$$[\mathbf{\Phi}]_{3\alpha+i-3,3\beta+j-3} = \left.\frac{\partial^2 U(\{\mathbf{x}^0\}+\{\mathbf{u}\})}{\partial \mathbf{u}_{\alpha i}\partial \mathbf{u}_{\beta j}}\right|_{\mathbf{u}=0} \quad \alpha,\beta = 1,\ldots,N, \quad i,j = 1,2,3. \tag{4}$$

By taking the harmonic time dependence for all the atoms, the equation of motion can be written as [14]

$$\left([\mathbf{\Phi}] - \omega^2[\mathbf{M}]\right)\{\mathbf{d}\} = 0 \tag{5}$$

where $\{\mathbf{d}\}$ is the normal mode vector and $[\mathbf{M}]$ is the $3N \times 3N$ mass matrix and ω is the phonon frequency of the system. Note that, while the masses of the filler and the matrix atoms are typically different, the mass matrix $[\mathbf{M}]$ is diagonal if the masses of the atoms are assumed to be concentrated. The phonon frequencies can be computed directly by solving the generalized eigen problem given in Eq. (5). Once the phonon frequencies ω are obtained, the PDOS can be readily obtained. Due to the fact that the $3N \times 3N$ eigen system must be solved in the direct approach, the computational cost can become very high when the system contains a large number of atoms. However, since the direct approach provides the "exact" solution of the PDOS, in this paper, the solution of the direct approach is used as reference for comparison with the results obtained from the MCMS.

2.2 Multilevel discretization

The first step of the MCMS is the multilevel discretization of the nanostructure. Figure 1 illustrates the basic idea of the multilevel discretization step in the MCMS approach by using a simple example: a cantilever nanostructure. The domain of the nanostructure is denoted by Ω. The nanostructure is discretized into 3 levels of substructures, as shown in Fig. 1. The j-th substructure in the m-th level is denoted by Ω_j^m, where $m = 1, 2, 3$, $j = 1, 2, \ldots, J_m$ and J_m is the total number of substructures in the m-th level. The top level is the nanostructure itself. Therefore, $\Omega_1^1 = \Omega$. The top-level nanostructure is discretized into eight second-level components, i.e., $J_2 = 8$. Each of the eight components is further discretized into four third-level substructures. The third level is the bottom level where the substructures are sufficiently small so that Eq. (5) can be directly solved with a small computational cost. Note that, although the nanostructure shown in Fig. 1 is divided into 3 levels of equal-size substructures, the number of levels and the size of the substructures can be arbitrary with the trade-off between the accuracy and efficiency of the solution. Discretization parameter studies are shown in Sect. 3.

The discretization of the nanostructure cuts through the center of the interface atoms, i.e., the atoms on the surface of a substructure are either on the boundary of the top-level nanostructure or shared by other substructures in the same level.

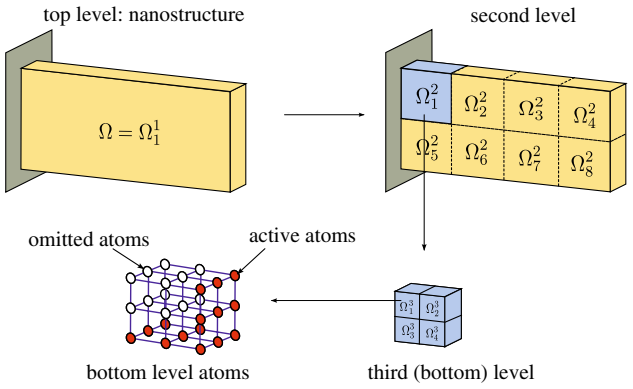

Fig. 1 Multilevel discretization

By using the terminology in the CMS literature, the atoms in each substructure are partitioned into two parts which are referred to as the active atoms and the omitted atoms. The active atoms are the atoms shared by connected substructures, and the omitted atoms are the atoms that are not active. For example, as shown in Fig. 1, the boundary atoms of substructure Ω_1^3 shared by neighboring third-level substructures are active atoms (shaded), and the remaining atoms in Ω_1^3 are omitted atoms (empty). The active and omitted atoms are denoted by subscripts a and o, respectively. The DOFs of the active and omitted atoms are called active and omitted DOFs and denoted by n_a and n_o, respectively.

2.3 Multilevel component mode synthesis

After the multilevel discretization, the MCMS procedure computes the phonon frequencies and modes of the substructures starting from the bottom level. In order to reduce the problem size, other than breaking the nanostructure into substructures, the CMS computes the phonon frequencies within a small preselected frequency band $[\omega_a, \omega_b]$ within the entire frequency spectrum $[0, \omega_{\max}]$, where $\omega_{\max}$ is the highest frequency obtained from the bottom-level substructures. In this paper, the frequency spectrum $[0, \omega_{\max}]$ is divided into 10 equal-width frequency bands, i.e., the width of each frequency band $[\omega_a, \omega_b]$ is a tenth of $\omega_{\max}$. The PDOS of the nanostructure is computed for each of the ten frequency bands. The computed PDOSs are then combined together to obtain the complete PDOS. In addition, the computed frequencies may fall outside of the frequency band $[\omega_a, \omega_b]$. Typically, the accuracy of the computed frequencies which are outside or near the boundary of the frequency band decreases. Therefore, for each preselected $[\omega_a, \omega_b]$, a slightly larger computational frequency band $[\omega_c, \omega_d]$ is used in the calculation. In this work, the center of the computational frequency band $[\omega_c, \omega_d]$ is set to be the center of $[\omega_a, \omega_b]$ and the width of $[\omega_c, \omega_d]$ is set to be $1.5 \times (\omega_b - \omega_a)$. The equation of motion for the vibrational modes of the j-th substructure

at the m-th level, $\left\{\mathbf{d}^{(m,j)}\right\}$, is give by Eq. (5), i.e.,

$$\left(\left[\mathbf{\Phi}^{(m,j)}\right]_{n\times n} - \omega^2\left[\mathbf{M}^{(m,j)}\right]_{n\times n}\right)\left\{\mathbf{d}^{(m,j)}\right\}_{n\times 1} = \{\mathbf{0}\}_{n\times 1}$$
$$m = 1, 2, \ldots, M, \quad j = 1, 2, \ldots, J_m, \tag{6}$$

where $[\mathbf{\Phi}]$ is the force constant matrix, $[\mathbf{M}]$ is the mass matrix, ω is the phonon frequency of the substructure Ω_j^m, the superscript (m, j) denotes the j-th substructure in the m-th level, M is the total number of discretization levels, and n is the DOFs of the substructure. In the MCMS approach, except for the bottom-level substructures, the vibrational modes $\left\{\mathbf{d}^{(m,j)}\right\}$ are not calculated by solving Eq. (6). Instead, $\left\{\mathbf{d}^{(m,j)}\right\}$ is approximated by a small set of selected component modes and the constraint modes [17], i.e.,

$$\left\{\mathbf{d}^{(m,j)}\right\}_{n\times 1} = \left\{\begin{array}{c}\mathbf{d}_o^{(m,j)}\\ \mathbf{d}_a^{(m,j)}\end{array}\right\}_{n\times 1} = \left[\begin{array}{cc}\bar{\mathbf{D}}_o^{(m,j)} & \mathbf{X}_o^{(m,j)}\\ \mathbf{0}_a & \mathbf{I}_a^{(m,j)}\end{array}\right]_{n\times r}\left\{\begin{array}{c}\mathbf{z}_r^{(m,j)}\\ \mathbf{d}_a^{(m,j)}\end{array}\right\}_{r\times 1}, \tag{7}$$

or in short form,

$$\left\{\mathbf{d}^{(m,j)}\right\}_{n\times 1} = \left[\mathbf{T}^{(m,j)}\right]_{n\times r}\left\{\mathbf{z}^{(m,j)}\right\}_{r\times 1}. \tag{8}$$

In Eq. (7), $\left\{\mathbf{d}^{(m,j)}\right\}$ is partitioned into omitted $\left\{\mathbf{d}_o^{(m,j)}\right\}$ and active $\left\{\mathbf{d}_a^{(m,j)}\right\}$ parts, the transformation matrix

$$\left[\mathbf{T}^{(m,j)}\right] = \left[\begin{array}{cc}\bar{\mathbf{D}}_o^{(m,j)} & \mathbf{X}_o^{(m,j)}\\ \mathbf{0}_a & \mathbf{I}_a\end{array}\right] \tag{9}$$

is comprised of n_r selected component modes given by $\left[\begin{array}{c}\bar{\mathbf{D}}_o^{(m,j)}\\ \mathbf{0}_a\end{array}\right]_{n\times n_r}$ and n_a constraint modes given by $\left[\begin{array}{c}\mathbf{X}_o^{(m,j)}\\ \mathbf{I}_a\end{array}\right]_{n\times n_a}$, where $\left[\bar{\mathbf{D}}_o^{(m,j)}\right]$ is the $n_o \times n_r$ reduced component modal matrix for the omitted atoms, $\left[\mathbf{X}_o^{(m,j)}\right]$ is the $n_o \times n_a$ constraint modal matrix for the omitted atoms, $[\mathbf{I}_a]$ is the identity matrix of the active atoms, and $[\mathbf{0}_a]$ is the null matrix. Note that, the identity matrix $[\mathbf{I}_a]$ represents the unit displacement of the active atoms in the constraint modes, and the null matrix $[\mathbf{0}_a]$ is the zero displacement of the active atoms in the component modes. The combined component and constraint modes are the $r = n_r + n_a << n$ Ritz basis vectors for $\left\{\mathbf{d}^{(m,j)}\right\}$. $\left\{\mathbf{z}^{(m,j)}\right\}$ in Eq. (8) is the generalized coordinate vector which can be partitioned into a component modal part, $\left\{\mathbf{z}_r^{(m,j)}\right\}$, and a constraint modal part, $\left\{\mathbf{d}_a^{(m,j)}\right\}$. As shown in Eq. (7), the constraint modal part of $\left\{\mathbf{z}^{(m,j)}\right\}$, $\left\{\mathbf{d}_a^{(m,j)}\right\}$, is precisely the active part of $\left\{\mathbf{d}^{(m,j)}\right\}$.

For a substructure Ω_j^m, the reduced component modal matrix, $\left[\bar{\mathbf{D}}_o^{(m,j)}\right]$, can be obtained from Eq. (6) with the active atoms held fixed. Equation (6) is partitioned with respect to the active and omitted DOFs as

$$\left(\left[\begin{array}{cc}\mathbf{\Phi}_{oo}^{(m,j)} & \mathbf{\Phi}_{oa}^{(m,j)}\\ \mathbf{\Phi}_{ao}^{(m,j)} & \mathbf{\Phi}_{aa}^{(m,j)}\end{array}\right] - \omega^2\left[\begin{array}{cc}\mathbf{M}_{oo}^{(m,j)} & \mathbf{M}_{oa}^{(m,j)}\\ \mathbf{M}_{ao}^{(m,j)} & \mathbf{M}_{aa}^{(m,j)}\end{array}\right]\right)\left\{\begin{array}{c}\mathbf{d}_o^{(m,j)}\\ \mathbf{d}_a^{(m,j)}\end{array}\right\} = \left\{\begin{array}{c}\mathbf{0}\\ \mathbf{0}\end{array}\right\} \tag{10}$$

By fixing the active atoms, i.e., $\{\mathbf{d}_a\} = \{\mathbf{0}\}$, we obtain

$$\left(\left[\mathbf{\Phi}_{oo}^{(m,j)}\right]_{n_o\times n_o} - \omega^2\left[\mathbf{M}_{oo}^{(m,j)}\right]_{n_o\times n_o}\right)\left\{\mathbf{d}_o^{(m,j)}\right\}_{n_o\times 1} = \{\mathbf{0}\}_{n_o\times 1} \tag{11}$$

The eigen pairs $\left(\omega, \left\{\mathbf{d}_o^{(m,j)}\right\}\right)$ can be computed from Eq. (11). The component modes for the omitted atoms, $\left\{\mathbf{d}_o^{(m,j)}\right\}$, can be assembled column-wise into the component modal matrix $\left[\mathbf{D}_o^{(m,j)}\right]$. In the MCMS, only the modes corresponding to the eigen frequencies inside the computational frequency band, i.e., $\omega_c \le \omega \le \omega_d$, are retained and the retained modes constitute the columns of $\left[\bar{\mathbf{D}}_o^{(m,j)}\right]$, i.e.,

$$\left[\bar{\mathbf{D}}_o^{(m,j)}\right] = \left\{\mathbf{d}_o^{(m,j)} : \omega_c \le \omega \; of \; \mathbf{d}_o^{(m,j)} \le \omega_d\right\} \tag{12}$$

Note that since the computational frequency band $[\omega_c, \omega_d]$ is a small part of the entire frequency spectrum, the number of retained modes is typically small compared to the total DOFs of Eq. (11). However, for a substructure with large DOFs, the computational cost of solving Eq. (11) can still be high. In the MCMS, Eq. (11) is only solved for the bottom-level substructures to obtain $\left[\bar{\mathbf{D}}_o^{(M,j)}\right]$. Since the DOFs of the bottom-level substructures is typically small, Eq. (11) can be solved efficiently. While the DOFs of the substructures in the upper levels becomes larger, Eq. (11) is not used to compute $\left[\bar{\mathbf{D}}_o^{(m,j)}\right]$. Instead, Eq. (7) is employed to obtain $\left[\bar{\mathbf{D}}_o^{(m,j)}\right]$. Thus, the higher computational cost of solving Eq. (11) for large substructures can be avoided in the MCMS. In the following paragraphs, we show that once $\left[\bar{\mathbf{D}}_o^{(m,j)}\right]$ is obtained $\left[\bar{\mathbf{D}}_o^{(m-1,j)}\right]$ can be computed efficiently without solving Eq. (11).

In the classical CMS, the constraint modal matrix is obtained by static analysis of the substructure with unit displacement prescribed on the active DOFs [17]. However, it has been shown [19] that the static constraint modes are only effective for obtaining the lowest frequencies of the system. For intermediate and high frequency bands, the static constraint modes may produce inaccurate results. In the MCMS, a quasi-static approach proposed in [19] is adopted in the calculation of the constraint modes. The quasi-static constraint

modes are derived from solving the equation of motion:

$$\left(\begin{bmatrix} \boldsymbol{\Phi}_{oo}^{(m,j)} & \boldsymbol{\Phi}_{oa}^{(m,j)} \\ \boldsymbol{\Phi}_{ao}^{(m,j)} & \boldsymbol{\Phi}_{aa}^{(m,j)} \end{bmatrix} - \omega_n^2 \begin{bmatrix} \mathbf{M}_{oo}^{(m,j)} & \mathbf{M}_{oa}^{(m,j)} \\ \mathbf{M}_{ao}^{(m,j)} & \mathbf{M}_{aa}^{(m,j)} \end{bmatrix}\right) \begin{bmatrix} \mathbf{X}_o^{(m,j)} \\ \mathbf{I}_a \end{bmatrix} = \begin{bmatrix} \mathbf{0} \\ \mathbf{R}_a^{(m,j)} \end{bmatrix} \tag{13}$$

where the $n_a \times n_a$ identity matrix $[\mathbf{I}_a]$ represents the boundary conditions applied to enforce unit vibrational displacement of each active DOF with other DOFs of the active atoms held fixed, $\{\mathbf{R}_a\}$ is the resultant reaction force vector at the active DOFs and ω_n is the center frequency of the computational frequency band $[\omega_c, \omega_d]$, i.e., $\omega_n = (\omega_c + \omega_d)/2$. The expression of the quasi-static constraint modal matrix $\left[\mathbf{X}_o^{(m,j)}\right]$ for the omitted atoms can be obtained from Eq. (13) explicitly as

$$\left[\mathbf{X}_o^{(m,j)}\right] = -\left(\left[\boldsymbol{\Phi}_{oo}^{(m,j)}\right] - \omega_n^2 \left[\mathbf{M}_{oo}^{(m,j)}\right]\right)^{-1} \times \left(\left[\boldsymbol{\Phi}_{oa}^{(m,j)}\right] - \omega_n^2 \left[\mathbf{M}_{oa}^{(m,j)}\right]\right) \tag{14}$$

Since $\left[\mathbf{M}^{(m,j)}\right]$ is diagonal, $[\mathbf{M}_{oa}^{(m,j)}] = [\mathbf{0}]$. Equation (14) can be rewritten as

$$\left[\mathbf{X}_o^{(m,j)}\right] = -\left(\left[\boldsymbol{\Phi}_{oo}^{(m,j)}\right] - \omega_n^2 \left[\mathbf{M}_{oo}^{(m,j)}\right]\right)^{-1} \left[\boldsymbol{\Phi}_{oa}^{(m,j)}\right] \tag{15}$$

Assuming that $\left[\bar{\mathbf{D}}_o^{(m,j)}\right]$ has already been obtained, by substituting $\left[\mathbf{X}_o^{(m,j)}\right]$ computed from Eq. (15) into Eq. (9), $\left[\mathbf{T}^{(m,j)}\right]$ can be obtained. Substituting Eq. (8) into Eq. (6), we obtain

$$\left(\left[\boldsymbol{\Phi}^{(m,j)}\right] - \omega^2 \left[\mathbf{M}^{(m,j)}\right]\right) \left[\mathbf{T}^{(m,j)}\right] \left\{\mathbf{z}^{(m,j)}\right\} = \{\mathbf{0}\} \tag{16}$$

Multiplying the transpose of $\left[\mathbf{T}^{(m,j)}\right]$ to both sides of Eq. (16), we obtain

$$\left[\mathbf{T}^{(m,j)}\right]^T \left(\left[\boldsymbol{\Phi}^{(m,j)}\right] - \omega^2 \left[\mathbf{M}^{(m,j)}\right]\right) \left[\mathbf{T}^{(m,j)}\right] \left\{\mathbf{z}^{(m,j)}\right\} = \{\mathbf{0}\} \tag{17}$$

Equation (17) can be rewritten in short form as

$$\left(\left[\bar{\boldsymbol{\Phi}}^{(m,j)}\right] - \omega^2 \left[\bar{\mathbf{M}}^{(m,j)}\right]\right) \left\{\mathbf{z}^{(m,j)}\right\} = \{\mathbf{0}\} \tag{18}$$

where

$$\left[\bar{\boldsymbol{\Phi}}^{(m,j)}\right] = \left[\mathbf{T}^{(m,j)}\right]^T \left[\boldsymbol{\Phi}^{(m,j)}\right] \left[\mathbf{T}^{(m,j)}\right] \tag{19}$$

and

$$\left[\bar{\mathbf{M}}^{(m,j)}\right] = \left[\mathbf{T}^{(m,j)}\right]^T \left[\mathbf{M}^{(m,j)}\right] \left[\mathbf{T}^{(m,j)}\right] \tag{20}$$

are the reduced component force constant and mass matrices for the j-th substructure in the m-th level. Following the standard assembly procedure, one can assemble Eq. (18) of the connected substructures into a global system of the parent substructure in the $(m-1)$-th level, i.e.,

$$\left(\left[\hat{\boldsymbol{\Phi}}^{(m-1,j)}\right] - \omega^2 \left[\hat{\mathbf{M}}^{(m-1,j)}\right]\right) \left\{\mathbf{z}^{(m-1,j)}\right\} = \{\mathbf{0}\} \tag{21}$$

where

$$\left[\hat{\boldsymbol{\Phi}}^{(m-1,j)}\right] = assemble\left(\left[\bar{\boldsymbol{\Phi}}^{(m,p)}, \bar{\boldsymbol{\Phi}}^{(m,p+1)}, \ldots, \bar{\boldsymbol{\Phi}}^{(m,q)}\right]\right),$$
$$\left[\hat{\mathbf{M}}^{(m-1,j)}\right] = assemble\left(\left[\bar{\mathbf{M}}^{(m,p)}, \bar{\mathbf{M}}^{(m,p+1)}, \ldots, \bar{\mathbf{M}}^{(m,q)}\right]\right),$$
$$\cup\{\Omega_p^m, \Omega_{p+1}^m, \ldots, \Omega_q^m\} = \Omega_j^{m-1} \tag{22}$$

The phonon frequencies ω and generalized coordinate vector $\left\{\mathbf{z}^{(m-1,j)}\right\}$ of the parent substructure can be computed by solving the eigen problem given in Eq. (21). The global transformation matrix of the parent substructure, $\left[\hat{\mathbf{T}}^{(m-1,j)}\right]$, can be obtained by assembling the transformation matrices of the child substructures, i.e.,

$$\left[\hat{\mathbf{T}}^{(m-1,j)}\right] = assemble\left(\left[\mathbf{T}^{(m,p)}, \mathbf{T}^{(m,p+1)}, \ldots, \mathbf{T}^{(m,q)}\right]\right),$$
$$\cup\{\Omega_p^m, \Omega_{p+1}^m, \ldots, \Omega_q^m\} = \Omega_j^{m-1} \tag{23}$$

Once $\left\{\mathbf{z}^{(m-1,j)}\right\}$ and $\left[\hat{\mathbf{T}}^{(m-1,j)}\right]$ are obtained, the phonon modes of the substructure Ω_j^{m-1}, $\left\{\mathbf{d}^{(m-1,j)}\right\}$, can then be computed by using Eq. (7), and $\left\{\mathbf{d}_o^{(m-1,j)}\right\}$ can be readily obtained from $\left\{\mathbf{d}^{(m-1,j)}\right\}$. The reduced modal matrix $\left[\bar{\mathbf{D}}_o^{(m-1,j)}\right]$ can then be obtained from the computed set of $\left\{\mathbf{d}_o^{(m-1,j)}\right\}$ by using Eq. (12). By repeating this procedure, the phonon frequencies, ω, and modes, $\{\mathbf{d}\}$, can be computed for the substructures in the levels $(m-2)$, $(m-3)$, …. This procedure continues until the phonon frequencies and modes of the top-level $(m=1)$ structure are obtained. Algorithm 1 summarizes the bottom-up multilevel component synthesis procedure.

3 Examples

In this section, several numerical examples are presented. In the first example, the MCMS methodology is illustrated explicitly for a simple 1-D monatomic chain. The MCMS is then applied to compute the PDOS for several 1-D and 2-D composite nanostructures. The nanocomposite structures in the examples are assumed to be two-phase systems. While the MCMS is a general approach independent of interatomic potentials, in this paper, for the purpose of demonstrating the computational approach, a Lennard-Jones potential is

Algorithm 1 Procedure of the bottom-up multilevel component synthesis

1: For a given computational frequency band, start from the bottom level, i.e., $m = M$;
2: **for** $m = M, M-1,\ldots,2$ **do**
3: **for** each substructure Ω_j^m in level m **do**
4: Construct and partition the force constant and mass matrices for the bottom-level substructures as shown in Eq. (10).
5: **if** Ω_j^m is a bottom-level substructure **then**
6: Compute the component normal modes $\left[\mathbf{D}_o^{(m,j)}\right]$, $m = M$, by using Eq. (11).
7: **else**
8: Assemble the reduced force constant, mass and transformation matrices computed from the component structures in the $(m+1)$-th level to obtain $\left[\hat{\mathbf{\Phi}}^{(m,j)}\right]$, $\left[\hat{\mathbf{M}}^{(m,j)}\right]$, $\left[\hat{\mathbf{T}}^{(m,j)}\right]$ by using Eqs. (22,23).
9: Compute the frequencies and the generalized coordinate vector $\left\{\mathbf{z}^{(m,j)}\right\}$ by using Eq. (21).
10: Compute the normal modes $\left\{\mathbf{d}^{(m,j)}\right\}$ by using Eq. (7).
11: **end if**
12: Obtain the reduced component modes, $\left[\bar{\mathbf{D}}_o^{(m,j)}\right]$, by using Eq. (12).
13: Compute the quasi-static constraint modes $\left[\mathbf{X}_o^{(m,j)}\right]$by using Eq. (15).
14: Obtain the transformation matrix $\left[\mathbf{T}^{(m,j)}\right]$ by using Eq. (9).
15: Compute the reduced component force constant and mass matrices, $\left[\bar{\mathbf{\Phi}}^{(m,j)}\right]$ and $\left[\bar{\mathbf{M}}^{(m,j)}\right]$ by using Eqs. (19,20), respectively.
16: **end for**
17: m=m-1.
18: **end for**

employed to model the interaction between the atoms, i.e.,

$$V(r_{ij}) = 4\epsilon\left[\left(\frac{\sigma}{r_{ij}}\right)^{12} - \left(\frac{\sigma}{r_{ij}}\right)^{6}\right] \tag{24}$$

where ϵ and σ are parameters. In the examples, different parameters are used for the interaction between two filler atoms, the interaction between two matrix atoms and the interaction between a filler atom and a matrix atom. For simplicity, the size and bond configuration of the filler atoms are assumed to be the same as the matrix atoms. In addition, nearest neighbor interaction is assumed for the computation.

3.1 1-D monatomic chain

In the first example, we illustrate the computational procedure of the MCMS by using a simple 11-atom monatomic chain. As shown in Fig. 2, the atom chain is fixed at both ends. For simplicity, a unit mass of the atoms and a unit stiffness of the bonds are assumed. The multi-level discretization of the atom chain is shown in Fig. 2. The atom chain is represented by 3 levels of substructures. The atom chain (top-level substructure) is discretized into two second-level substructures, and the first second-level substructure is further

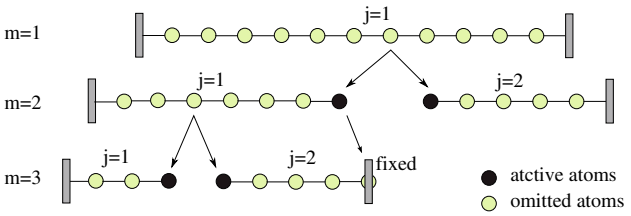

Fig. 2 MCMS discretization for a 1-D atom chain

discretized into two third-level substructures. In the discretization of the top-level atom chain, the 7-th atom is split into two active atoms of the two second-level substructures. Each of the active atoms has half of the original atom mass and a free boundary condition. In the discretization of Ω_1^2, the third atom is split into two third-level active atoms. The active atom in Ω_1^2 becomes a fixed atom in Ω_2^3. In the MCMS hierarchical discretization, it is not required that all the branches have the same levels of substructures. In this example, the substructure Ω_2^2 is not discretized further. Therefore, although Ω_2^2 is in level 2, it is a bottom-level substructure. The bottom-level substructures Ω_1^3, Ω_2^3 and Ω_2^2 contain 3,4 and 5 atoms, respectively. For illustration purpose, the entire frequency spectrum is divided into 2 equal-width frequency bands, from 0 to the highest frequency obtained from the bottom-level solution. In this case, Ω_2^2 gives the highest bottom-level substructure frequency of 1.902 rad/s. Therefore, the two frequency bands, $[\omega_a, \omega_b]$, are set to be $[0,\ 0.951]$ and $[0.951,\ 1.902]$, and their corresponding computational frequency bands, $[\omega_c, \omega_d]$, are set to be $[0,\ 1.189]$ and $[0.713,\ 2.140]$, respectively. In the following, we calculate the frequencies of the atom chain within the first frequency band.

By following Algorithm 1, we first construct and partition the force constant and mass matrices for the bottom-level substructures as shown in Eq. (10). The partitioned force constant and mass matrices are obtained as

$$\left[\mathbf{\Phi}^{(3,1)}\right] = \left[\begin{array}{cc|c} 2.0 & -1.0 & 0 \\ -1.0 & 2.0 & -1.0 \\ \hline 0 & -1.0 & 1.0 \end{array}\right]$$

$$\left[\mathbf{M}^{(3,1)}\right] = \left[\begin{array}{cc|c} 1.0 & 0 & 0 \\ 0 & 1.0 & 0 \\ \hline 0 & 0 & 0.5 \end{array}\right] \tag{25}$$

$$\left[\mathbf{\Phi}^{(3,2)}\right] = \left[\begin{array}{c|ccc} 1.0 & -1.0 & 0 & 0 \\ \hline -1.0 & 2.0 & -1.0 & 0 \\ 0 & -1.0 & 2.0 & -1.0 \\ 0 & 0 & -1.0 & 2.0 \end{array}\right]$$

$$\left[\mathbf{M}^{(3,2)}\right] = \left[\begin{array}{c|ccc} 0.5 & 0 & 0 & 0 \\ \hline 0 & 1.0 & 0 & 0 \\ 0 & 0 & 1.0 & 0 \\ 0 & 0 & 0 & 1.0 \end{array}\right] \tag{26}$$

$$\left[\mathbf{\Phi}^{(2,2)}\right] = \left[\begin{array}{c|cccc} 1.0 & -1.0 & 0 & 0 & 0 \\ \hline -1.0 & 2.0 & -1.0 & 0 & 0 \\ 0 & -1.0 & 2.0 & -1.0 & 0 \\ 0 & 0 & -1.0 & 2.0 & -1.0 \\ 0 & 0 & 0 & -1.0 & 2.0 \end{array}\right]$$

$$\left[\mathbf{M}^{(2,2)}\right] = \left[\begin{array}{c|cccc} 0.5 & 0 & 0 & 0 & 0 \\ \hline 0 & 1.0 & 0 & 0 & 0 \\ 0 & 0 & 1.0 & 0 & 0 \\ 0 & 0 & 0 & 1.0 & 0 \\ 0 & 0 & 0 & 0 & 1.0 \end{array}\right] \tag{27}$$

Note that the largest blocks in the partitioned force constant and mass matrices shown above are the $\left[\mathbf{\Phi}_{oo}^{(m,j)}\right]$ and $\left[\mathbf{M}_{oo}^{(m,j)}\right]$ matrices. For the 3 bottom-level substructures, the component frequencies and modes for the omitted atoms are calculated by using Eq. (11) as

$$\boldsymbol{\omega}^{(3,1)} = \left\{\begin{array}{c} 1.000 \\ 1.732 \end{array}\right\}$$

$$\left[\mathbf{D}_o^{(3,1)}\right] = \left[\begin{array}{cc} -0.707 & -0.707 \\ -0.707 & 0.707 \end{array}\right] \tag{28}$$

$$\boldsymbol{\omega}^{(3,2)} = \left\{\begin{array}{c} 0.765 \\ 1.414 \\ 1.848 \end{array}\right\}$$

$$\left[\mathbf{D}_o^{(3,2)}\right] = \left[\begin{array}{ccc} -0.500 & -0.707 & 0.500 \\ -0.707 & 0 & -0.707 \\ -0.500 & 0.707 & 0.500 \end{array}\right] \tag{29}$$

$$\boldsymbol{\omega}^{(2,2)} = \left\{\begin{array}{c} 0.618 \\ 1.176 \\ 1.618 \\ 1.902 \end{array}\right\}$$

$$\left[\mathbf{D}_o^{(2,2)}\right] = \left[\begin{array}{cccc} -0.372 & 0.602 & 0.602 & -0.372 \\ -0.602 & 0.372 & -0.372 & 0.602 \\ -0.602 & -0.372 & -0.372 & -0.602 \\ -0.372 & -0.602 & 0.602 & 0.372 \end{array}\right] \tag{30}$$

In each component modal matrix, we neglect the modes corresponding to the frequencies that fall out of the computational frequency band, [0, 1.189]. The retained modes for the bottom-level substructures are obtained using Eq. (12),

$$\left[\bar{\mathbf{D}}_o^{(3,1)}\right] = \left[\begin{array}{c} -0.707 \\ -0.707 \end{array}\right]$$

$$\left[\bar{\mathbf{D}}_o^{(3,2)}\right] = \left[\begin{array}{c} -0.500 \\ -0.707 \\ -0.500 \end{array}\right] \tag{31}$$

$$\left[\bar{\mathbf{D}}_o^{(2,2)}\right] = \left[\begin{array}{cc} -0.372 & 0.602 \\ -0.602 & 0.372 \\ -0.602 & -0.372 \\ -0.372 & -0.602 \end{array}\right]$$

By using the partitions of the force constant and mass matrices obtained in Eqs. (25–27) and the center frequency of $\omega_n = 0.476$, the quasi-static constraint modes of the bottom-level substructures are calculated by using Eq. (15),

$$\left[\mathbf{X}_o^{(3,1)}\right] = \left[\begin{array}{c} 0.466 \\ 0.827 \end{array}\right] \qquad \left[\mathbf{X}_o^{(3,2)}\right] = \left[\begin{array}{c} 1.056 \\ 0.873 \\ 0.492 \end{array}\right]$$

$$\left[\mathbf{X}_o^{(2,2)}\right] = \left[\begin{array}{c} 1.395 \\ 1.473 \\ 1.218 \\ 0.687 \end{array}\right] \tag{32}$$

The transformation matrices $\left[\mathbf{T}^{(m,j)}\right]$ can then be easily obtained by using Eq. (9),

$$\left[\mathbf{T}^{(3,1)}\right] = \left[\begin{array}{cc} -0.707 & 0.466 \\ -0.707 & 0.827 \\ 0 & 1.0 \end{array}\right]$$

$$\left[\mathbf{T}^{(3,2)}\right] = \left[\begin{array}{cc} 1.0 & 0 \\ 1.056 & -0.500 \\ 0.873 & -0.707 \\ 0.492 & -0.500 \end{array}\right] \tag{33}$$

$$\left[\mathbf{T}^{(2,2)}\right] = \left[\begin{array}{ccc} 1.0 & 0 & 0 \\ 1.395 & -0.372 & 0.602 \\ 1.473 & -0.602 & 0.372 \\ 1.218 & -0.602 & -0.372 \\ 0.687 & -0.372 & -0.602 \end{array}\right] \tag{34}$$

The reduced force constant and mass matrices are computed from Eqs. (19,20) as

$$\left[\bar{\mathbf{\Phi}}^{(3,1)}\right] = \left[\begin{array}{cc} 1.000 & -0.207 \\ -0.207 & 0.377 \end{array}\right]$$

$$\left[\bar{\mathbf{M}}^{(3,1)}\right] = \left[\begin{array}{cc} 1.000 & -0.914 \\ -0.914 & 1.401 \end{array}\right] \tag{35}$$

$$\left[\bar{\mathbf{\Phi}}^{(3,2)}\right] = \left[\begin{array}{cc} 0.424 & -0.315 \\ -0.315 & 0.586 \end{array}\right]$$

$$\left[\bar{\mathbf{M}}^{(3,2)}\right] = \left[\begin{array}{cc} 2.621 & -1.392 \\ -1.392 & 1.000 \end{array}\right] \tag{36}$$

$$\left[\bar{\mathbf{\Phi}}^{(2,2)}\right] = \left[\begin{array}{ccc} 0.981 & -0.542 & 0.118 \\ -0.542 & 0.382 & 0 \\ 0.118 & 0 & 1.382 \end{array}\right]$$

$$\left[\bar{\mathbf{M}}^{(2,2)}\right] = \left[\begin{array}{ccc} 6.570 & -2.392 & 0.521 \\ -2.392 & 1.000 & 0 \\ 0.521 & 0 & 1.000 \end{array}\right] \tag{37}$$

The reduced force constant matrices $\left(\left[\bar{\mathbf{\Phi}}^{(3,1)}\right], \left[\bar{\mathbf{\Phi}}^{(3,2)}\right]\right)$ and the reduced mass matrices $\left(\left[\bar{\mathbf{M}}^{(3,1)}\right], \left[\bar{\mathbf{M}}^{(3,2)}\right]\right)$ of the

two third-level substructures are then assembled as shown in Eq. (22),

$$\left[\hat{\mathbf{\Phi}}^{(2,1)}\right] = \begin{bmatrix} 1.000 & -0.207 & 0 \\ -0.207 & 0.802 & -0.315 \\ 0 & -0.315 & 0.586 \end{bmatrix}$$
$$\left[\hat{\mathbf{M}}^{(2,1)}\right] = \begin{bmatrix} 1.000 & -0.914 & 0 \\ -0.914 & 4.022 & -1.392 \\ 0 & -1.392 & 1.000 \end{bmatrix} \quad (38)$$

The transformation matrices ($\left[\mathbf{T}^{(3,1)}\right]$, $\left[\mathbf{T}^{(3,2)}\right]$) are assembled into a global transformation matrix by using Eq. (23),

$$\left[\hat{\mathbf{T}}^{(2,1)}\right] = \begin{bmatrix} -0.707 & 0.466 & 0 \\ -0.707 & 0.827 & 0 \\ 0 & 1.000 & 0 \\ 0 & 1.056 & -0.500 \\ 0 & 0.873 & -0.707 \\ 0 & 0.492 & -0.500 \end{bmatrix} \quad (39)$$

The eigen frequencies and the generalized coordinate vector, $\left\{\mathbf{z}^{(2,1)}\right\}$, for the substructure Ω_1^2 can be obtained from Eq. (21),

$$\boldsymbol{\omega}^{(2,1)} = \begin{Bmatrix} 0.445 \\ 0.869 \\ 1.359 \end{Bmatrix}$$
$$\left[\mathbf{z}^{(2,1)}\right] = \begin{bmatrix} -0.032 & 0.406 & 0.649 \\ -0.994 & -0.205 & 0.371 \\ -0.102 & -0.890 & 0.664 \end{bmatrix} \quad (40)$$

The component modes of the substructure Ω_1^2, $\left[\mathbf{D}_o^{(2,1)}\right]$, can be calculated by using Eq. (7). The reduced component modes, $\left[\bar{\mathbf{D}}_o^{(2,1)}\right]$, are then obtained by selecting the component modes in $\left[\mathbf{D}_o^{(2,1)}\right]$ with respect to the computed eigen frequencies and the computational frequency band as shown in Eq. (12), i.e.,

$$\left[\mathbf{D}_o^{(2,1)}\right] = \left[\hat{\mathbf{T}}^{(2,1)}\right]\left[\mathbf{z}^{(2,1)}\right] = \begin{bmatrix} -0.441 & -0.383 & -0.286 \\ -0.799 & -0.457 & -0.152 \\ -0.994 & -0.205 & 0.371 \\ -0.999 & 0.228 & 0.060 \\ -0.796 & 0.450 & -0.145 \\ -0.439 & 0.344 & -0.149 \end{bmatrix}$$
$$\left[\bar{\mathbf{D}}_o^{(2,1)}\right] = \begin{bmatrix} -0.441 & -0.383 \\ -0.799 & -0.457 \\ -0.994 & -0.205 \\ -0.999 & 0.228 \\ -0.796 & 0.450 \\ -0.439 & 0.344 \end{bmatrix} \quad (41)$$

Note that, as shown in Eq. (41), the component modes of the upper-level substructure Ω_1^2 are not directly computed by solving Eq. (11), which can be expensive if the substructure contains many DOFs. In the MCMS, the upper-level component modes are computed more efficiently from the results obtained from the lower-level substructures. The quasi-static constraint modes of Ω_1^2, $\left[\mathbf{X}_o^{(2,1)}\right]$, are computed by using Eq. (15) in the same manner as the bottom-level substructures. Combining $\left[\mathbf{X}_o^{(2,1)}\right]$ with the retained component modes calculated in Eq. (41), the transformation matrix $\left[\mathbf{T}^{(2,1)}\right]$ can be obtained from Eq. (9). In this example, $\left[\mathbf{X}_o^{(2,1)}\right]$ and $\left[\mathbf{T}^{(2,1)}\right]$ are obtained as

$$\left[\mathbf{X}_o^{(2,1)}\right] = \begin{bmatrix} -2.093 \\ -3.712 \\ -4.490 \\ -4.251 \\ -3.048 \\ -1.155 \end{bmatrix}$$
$$\left[\mathbf{T}^{(2,1)}\right] = \begin{bmatrix} -0.441 & -0.382 & -2.093 \\ -0.799 & -0.457 & -3.712 \\ -0.994 & -0.205 & -4.490 \\ -0.999 & 0.228 & -4.251 \\ -0.796 & 0.450 & -3.048 \\ -0.439 & 0.344 & -1.155 \\ 0 & 0 & 1 \end{bmatrix} \quad (42)$$

The reduced force constant and mass matrices of Ω_1^2 are computed from Eqs. (19,20) as

$$\left[\bar{\mathbf{\Phi}}^{(2,1)}\right] = \begin{bmatrix} 0.722 & 0 & 3.520 \\ 0 & 0.582 & 0.154 \\ 3.520 & 0.154 & 17.340 \end{bmatrix}$$
$$\left[\bar{\mathbf{M}}^{(2,1)}\right] = \begin{bmatrix} 3.647 & 0 & 15.537 \\ 0 & 0.771 & 0.678 \\ 15.537 & 0.678 & 67.519 \end{bmatrix} \quad (43)$$

Assembling the reduced force constant and mass matrices of Ω_1^2 and Ω_2^2 given in Eqs. (43, 37), the reduced system of the top-level atom chain is obtained, i.e.,

$$\left[\hat{\mathbf{\Phi}}^{(1,1)}\right] = \begin{bmatrix} 0.722 & 0 & 3.520 & 0 & 0 \\ 0 & 0.582 & 0.154 & 0 & 0 \\ 3.520 & 0.154 & 18.320 & -0.542 & 0.118 \\ 0 & 0 & -0.542 & 0.382 & 0 \\ 0 & 0 & 0.118 & 0 & 1.382 \end{bmatrix} \quad (44)$$

$$\left[\hat{\mathbf{M}}^{(1,1)}\right] = \begin{bmatrix} 3.647 & 0 & 15.537 & 0 & 0 \\ 0 & 0.771 & 0.678 & 0 & 0 \\ 15.537 & 0.678 & 74.088 & -2.392 & 0.521 \\ 0 & 0 & -2.392 & 1.0 & 0 \\ 0 & 0 & 0.521 & 0 & 1.0 \end{bmatrix} \quad (45)$$

The eigen frequencies of the top-level atom chain can be obtained by solving Eq. (21) using the reduced force con-

Table 1 Comparison of the eigen frequencies obtained from the MCMS and the direct approaches

Freq.	MCMS		Direct
ω_1	1st freq. band	0.261847	0.261052
ω_2		0.517707	0.517638
ω_3		0.769515	0.765367
ω_4	2nd freq. band	0.992882	1.000000
ω_5		1.217441	1.217523
ω_6		1.414211	1.414214
ω_7		1.586682	1.586707
ω_8		1.731214	1.732051
ω_9		1.846841	1.847759
ω_{10}		1.931241	1.931852
ω_{11}		1.980417	1.982890

stant and mass matrices given in Eqs. (44,45), i.e.,

$$\boldsymbol{\omega}^{(1,1)} = \begin{Bmatrix} 0.261847 \\ 0.517707 \\ 0.769515 \\ 1.012656 \\ 1.370292 \end{Bmatrix} \tag{46}$$

Since the first frequency band is [0, 0.902], we only keep the calculated frequencies within this frequency band, i.e., $\boldsymbol{\omega} = \{0.261847,\ 0.517707,\ 0.769515\}^T$. This calculation procedure is repeated for the second frequency band. Table 1 summarizes the results obtained from the MCMS approach compared with the results from the direct approach. It is shown in the table that the MCMS results are quite accurate and the maximum error in the eigen frequencies is within 0.8% of the "exact" solution obtained from the direct approach.

3.2 1-D composite atom chain

The second example is an 1-D composite atom chain fixed at the two ends. The total number of atoms is 1,601 (including both the filler and matrix atoms). There are 32 nanoparticles uniformly distributed in the atom chain. Each nanoparticle is comprised of ten filler atoms. The masses of the matrix and filler atoms are set to be 2×10^{-26} and 8×10^{-26} kg, respectively. The coefficients in the Lennard-Jones potential for the interaction between two matrix atoms are set to be $\epsilon = 0.2$ eV and $\sigma = 0.3$ nm with an equilibrium bond length of 0.337 nm. For the interaction between two filler atoms, we set $\epsilon = 0.153$ eV and $\sigma = 0.25$ nm with an equilibrium bond length of 0.281 nm. For the interaction between a matrix atom and a filler atom at the material interface, we set $\epsilon = 0.48$ eV and $\sigma = 0.38$ nm with an equilibrium bond length of 0.427 nm. As described in Sect. 2, in the MCMS calculation, the entire frequency spectrum is divided into ten equal-width frequency bands, from 0 to the highest frequency obtained from the bottom-level solution.

In the PDOS calculations by using the MCMS approach, one can choose various substructure discretization schemes with different discretization levels and substructure sizes. In this example, we show the effect of the discretization schemes on the accuracy and efficiency of the MCMS approach. We discretize the entire atom chain by using 11 schemes. In Scheme 1, the atom chain is discretized into 5 levels of substructures: the top level is the atom chain itself which is discretized into two second-level substructures each containing 801 atoms; each second-level substructure is then discretized into 2 third-level substructures of 401 atoms, and so on so forth. Each of the bottom-level (the fifth level) substructures contains 101 atoms. In Scheme 2, we discretize the atom chain in the same manner as described in Scheme 1 except that the discretization stops at the fourth level. Therefore, each of the bottom-level substructures in Scheme 2 contains 201 atoms. We repeat the same procedure in Scheme 3 and stop at the third level. In Scheme 4, each upper-level substructure is discretized into four equal-size lower-level substructures, i.e., the atom chain is discretized into four second-level substructures each containing 401 atoms and each second-level substructure is then discretized into four third-level (bottom-level) substructures of 101 atoms. In Schemes 5–8, we choose a two-level description of the atom chain and discretize the atom chain into 2, 4, 8 and 16 equal-size second-level substructures, respectively. In Schemes 9–11, the top-level atom chain is discretized into two second-level substructures with the ratio between the substructure sizes varying from 1:15 to 1:3. The schemes are summarized in Table 2.

The PDOS of the composite atom chain is calculated by using the 11 MCMS schemes. Very accurate PDOS results are observed for all the MCMS schemes. Figure 3 shows the atom configuration of the 1-D atom chain and the PDOS obtained by using the direct method and the MCMS with Scheme 1. The PDOS obtained from the MCMS is almost identical to that obtained by using the direct method. The PDOS plots obtained from other discretization schemes are indistinguishable from the curves shown in Fig. 3. For the clarity of the figure, these plots are not shown. Although all the 11 MCMS schemes give very accurate PDOS of the composite atom chain, small errors exist for individual eigen frequencies. Figure 4 shows the eigen frequencies within the frequency band [7.098 THz, 8.112 THz] obtained from Schemes 5 (2 levels), 3 (3 levels), 2 (4 levels) and 1 (5 levels) compared with the direct solution. The MCMS schemes give identical number of eigen frequencies within the frequency band. However, as shown in Fig. 4, the eigen frequencies obtained from the MCMS schemes are slightly different from the exact solution near the ends of the frequency band. From the inset

Table 2 Computational cost comparison of various MCMS discretization schemes and the direct approach

Approach	Discretization scheme				CPU time (s)
	Scheme ID	Levels	Number of substructures (from top level to bottom level)	Substructure sizes (atoms)	
MCMS	1	5	1→ 2→ 4→ 8→16	1,601→ 2 × 801→ 4 × 401 → 8 × 201 → 16 × 101	83
	2	4	1→ 2→ 4→8	1,601→ 2 × 801→ 4 × 401 → 8 × 201	121
	3	3	1→ 2→ 4	1,601→ 2 × 801→ 4 × 401	155
	4		1→ 4→ 16	1,601→ 4×401 → 16 × 101	19
	5	2	1→ 2	1,601→ 2 × 801	294
	6		1→ 4	1,601→ 4 × 401	62
	7		1→ 8	1,601→ 8 × 201	26
	8		1→ 16	1,601→ 16 × 101	11
	9		1→2	1,601 → 101 + 1,501	1,087
	10		1→2	1,601 → 201 + 1,401	930
	11		1→2	1,601 → 401 + 1,201	534
Direct		1	1	1,601	54

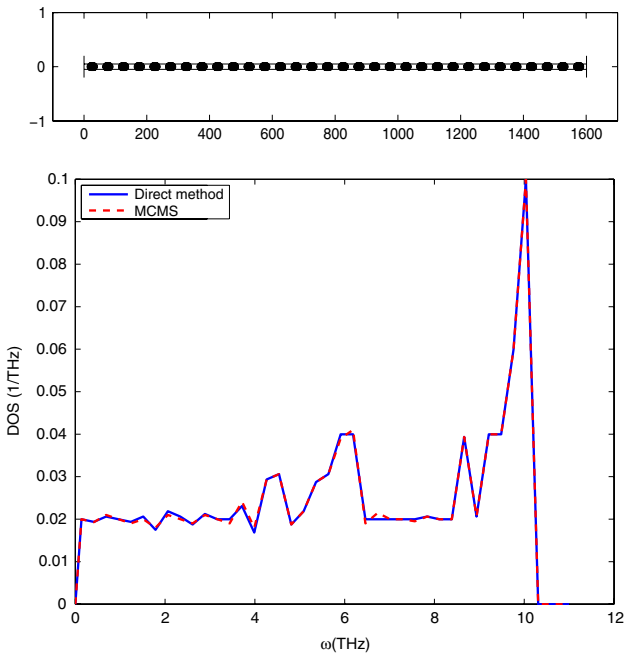

Fig. 3 PDOS of a 1-D composite atom chain with a uniform distribution of the filler nanoparticles

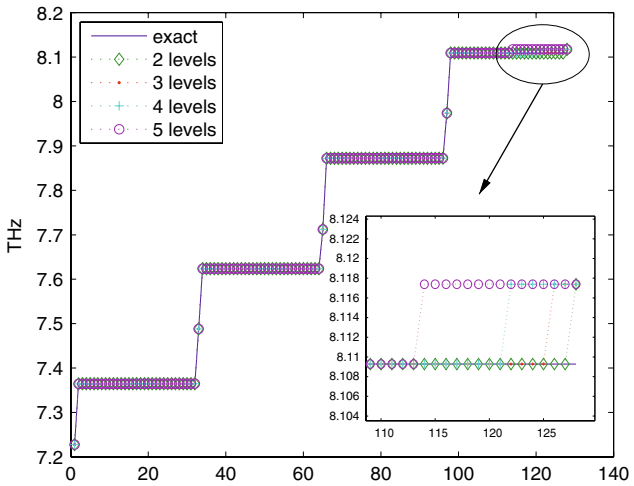

Fig. 4 Comparison of the eigen frequencies obtained from different MCMS discretization schemes

of Fig. 4, we observe that the number of frequencies that are off from the exact solution increases as the discretization levels increase. This implies that, as the discretization levels increase, the MCMS results can be less accurate, although the error is within 0.1% of the direct solution and is only observed near the ends of the frequency band.

The computational cost of the 11 MCMS schemes is listed in Table 2. The calculations show that, when all the other discretization parameters are kept the same, reducing discretization levels from 5 levels to 2 levels causes an increase in computational cost from 83 to 294 s in this case (compare Schemes 1–3 and 5 in Table 2). Comparing the CPU time for Schemes 5–8 shows that the computational cost can be reduced by discretizing a substructure into many lower-level substructures. However, as will be shown in Sect. 3.3, this may not be true in other cases. When a substructure is discretized into many substructures, the number of active atoms that

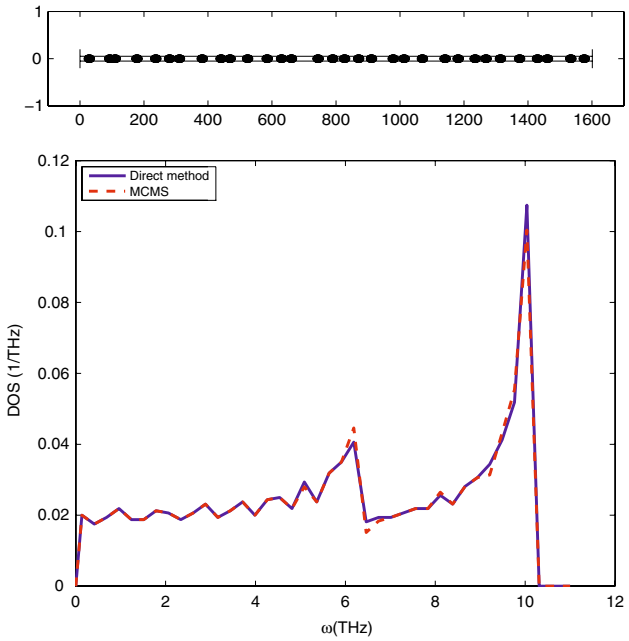

Fig. 5 PDOS of a 1-D composite atom chain with a pseudo random distribution of the filler nanoparticles

are shared by lower-level substructures can become large. Since the DOFs of the active atoms are included in the calculations, a large number of active DOFs can significantly increase the computational cost. The CPU time results for Schemes 9–11 show that when a substructure is discretized into lower-level substructures with a high size ratio, the computational cost increases significantly. This is due to the fact that the computational cost is dominated by the larger substructure. Therefore, discretizing the substructures into similar sized lower-level substructures is recommended to obtain a balanced efficiency of the computational analysis. Note that, in this example, the CPU time of the direct approach is 54 s. As shown in Table 2, only MCMS Schemes 4, 7 and 8 are more efficient than the direct approach in this case. This result shows that, when the DOFs of the system is small, the efficiency of the MCMS is not significant due to the overhead of the matrix operations.

The third example is an 1-D composite atom chain with a pseudo random distribution of 32 filler nanoparticles. All the other parameters used in the calculation are the same as those used in the second example. The atom chain is discretized by using Scheme 1 described in the second example. The pseudo random distribution of the filler nanoparticles is generated by a random perturbation of the positions of the uniformly distributed nanoparticles. Figure 5 shows the atom configuration of the 1-D atom chain and the PDOS obtained by using the direct method and the MCMS. As shown in Fig. 5, due to the splitting of the degenerate phonon modes, the high frequency part of the PDOS of the atom chain with randomly distributed nanoparticles shows a significant change compared to the PDOS of the atom chain with uniformly distributed nanoparticles. It is shown that the MCMS accurately reproduces the PDOS of the composite atom chain.

3.3 2-D composite atom sheet

In the fourth example, the MCMS is applied to calculate the PDOS of a square atom sheet. Figure 6a shows the configuration of the atoms. The square sheet contains 81×81 atoms. The top and right edges of the square sheet are fixed. The left and bottom edges of the atom sheet are free. There are 64 (8×8) nanoparticles uniformly distributed in the atom sheet. Each nanoparticle is comprised of 12 filler atoms as shown in Fig. 6a. The masses of the matrix and filler atoms are set to be 2×10^{-26} and 1×10^{-26} kg, respectively. The coefficients of the Lennard-Jones potential for the interaction between two matrix atoms are set to be $\epsilon = 0.2$ eV and $\sigma = 0.3$ nm. For the interaction between two filler atoms, we set $\epsilon = 0.146$ eV and $\sigma = 0.27$ nm. For the interaction between a matrix atom and a filler atom at the material interface, we set $\epsilon = 0.14$ eV and $\sigma = 0.28$ nm. The atom sheet is discretized into four levels: one top-level 81×81-atom structure, four 41×41-atom second-level substructures, 16 (21×21)-atom third-level substructures and 64 (11×11)-atom fourth-level (bottom-level) substructures. The frequency spectrum is again divided into ten equal-width frequency bands in the MCMS. Figure 6b shows the comparison of the PDOS obtained from the direct and the MCMS approaches. The PDOS obtained from the MCMS is very close to that obtained by using the direct method. In this example, the CPU time of the direct method is 11,235 s and the total computational cost of the MCMS is 538 s. To obtain the computational cost as a function of the system size for the two approaches, the PDOS is calculated for two additional square atom sheets with 21×21 and 41×41 atoms. The 21×21 and the 41×41 atom sheets contain four and 16 uniformly distributed nanoparticles, respectively. The MCMS discretizes the 21×21 and the 41×41 atom sheets into 2 and 3 levels, respectively. The computational cost of the direct and MCMS approaches is summarized in Table 3. It is again shown that, when the DOFs of the system is small, the efficiency of the MCMS is not significant due to the overhead of the matrix operations in the MCMS. However, for large systems, the computational cost is largely reduced by using the MCMS. The reduction of the CPU time becomes larger as the system size grows. To further reduce the computational cost, one could discretize an upper-level substructure into more smaller size lower-level substructures. However, as discussed in the second example, a large number of lower-level substructures discretized from an upper-level substructure can introduce a large number of active DOFs and cause higher computational cost. In this example, we discretize the atom sheet into

Table 3 Computational cost comparison of the direct and the MCMS approaches

Atoms	DOFs	CPU time of the direct approach (s)	CPU time of the MCMS approach (s)
21×21	882	5.12	4.5
41×41	3,362	198	52
81×81	13,122	11,235	538

2 levels and compare the computational cost of the discretization schemes with different number of substructures. As shown in Table 4, when the atom sheet is discretized into 16 (21 × 21)-atom substructures, the CPU time is 1,785 s. The CPU time increases to 2,221 s when the atom sheet is discretized into 64 (11 × 11)-atom substructures. Both are larger than the CPU time of the 4-level discretization.

The fifth example is a 2-D composite atom sheet with a pseudo random distribution of 64 filler nanoparticles, as shown in Fig. 7a. All the other parameters used in the calculation are the same as those used in the third example. In this example, the CPU time of the direct method is 10,370 s and the total computational cost of the MCMS is 391 s. As shown in Fig. 7b, the PDOS obtained from the MCMS approach once again accurately reproduces the result obtained from the direct approach with a much less computational cost. The effect of the random distribution of the nanoparticles is clearly shown by comparing the PDOS in Figs. 6b and 7b.

The last example is an "L"-shaped 2-D nanostructure containing 104 pseudo randomly distributed nanoparticles. The total number of atoms is 10,400. In the MCMS, the structure is discretized into four levels. The multilevel discretization and the boundary conditions of the structure is shown in Fig. 8. In this example, the masses of the matrix and filler atoms are set to be 2×10^{-26} and 8×10^{-26} kg, respectively. The coefficients in the Lennard-Jones potential are set to be the same as those in the third and the fourth examples. Figure 9 shows the PDOS obtained from the direct and the MCMS approaches. The MCMS once again provides a very accurate result. The CPU time of the direct approach is 46,986 s while the MCMS requires 1,611 s, which is about 30 times faster than the direct approach.

4 Conclusion

In this paper, a multilevel component mode synthesis approach is presented for the calculations of the PDOS of nanocomposite structures. In this approach, nanocomposite structures are discretized into multiple levels of substructures in a top-down manner. For a given frequency band, the phonon frequencies and modes are first computed for the bottom-level substructures. The obtained component modes are then synthesized by using a quasi-static CMS technique to obtain the phonon frequencies and modes of upper-level

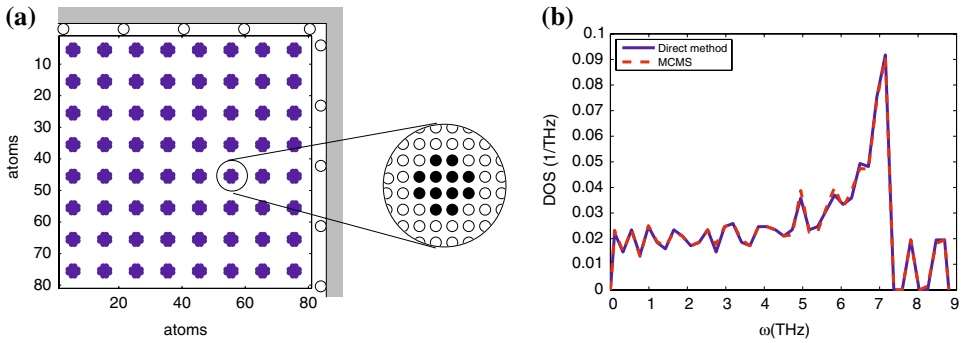

Fig. 6 **a** A square atom sheet containing uniformly distributed filler nanoparticles. **b** PDOS of the square atom sheet

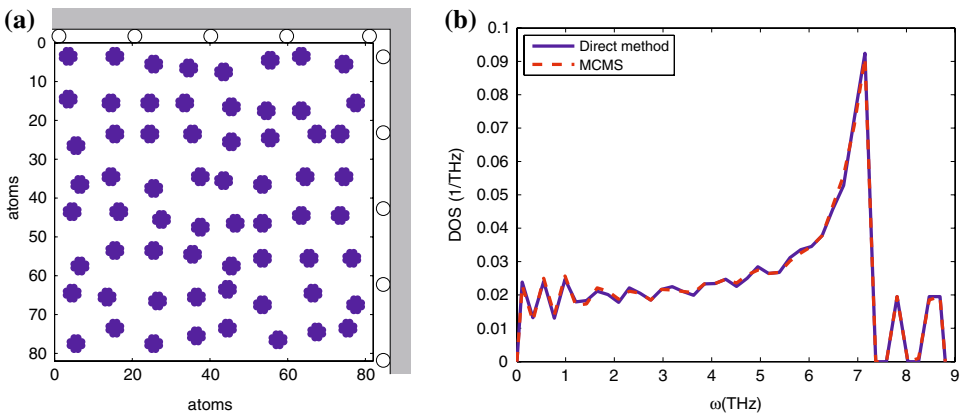

Fig. 7 **a** A square atom sheet with a pseudo random distribution of the filler nanoparticles. **b** PDOS of the square atom sheet

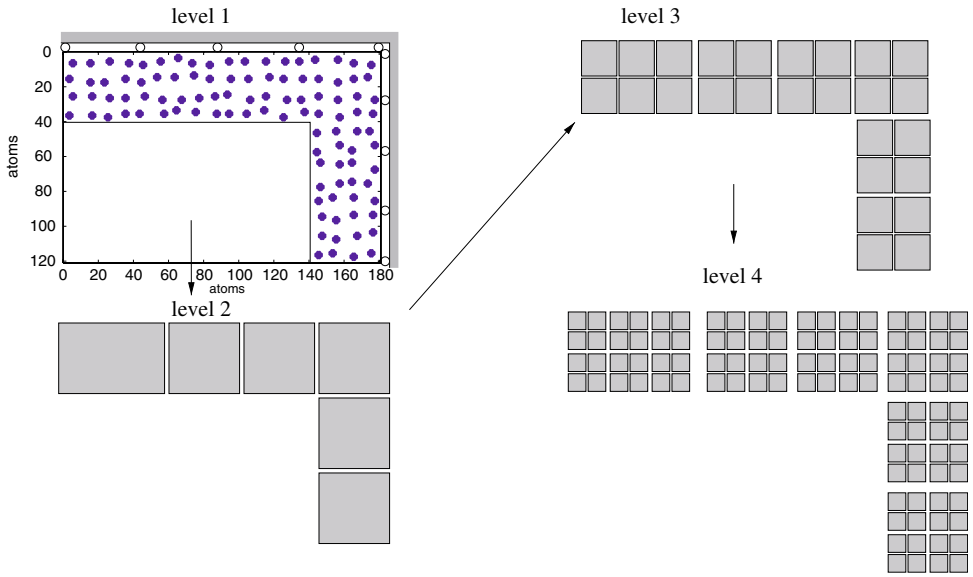

Fig. 8 Multilevel discretization of an "L"-shaped composite atom sheet

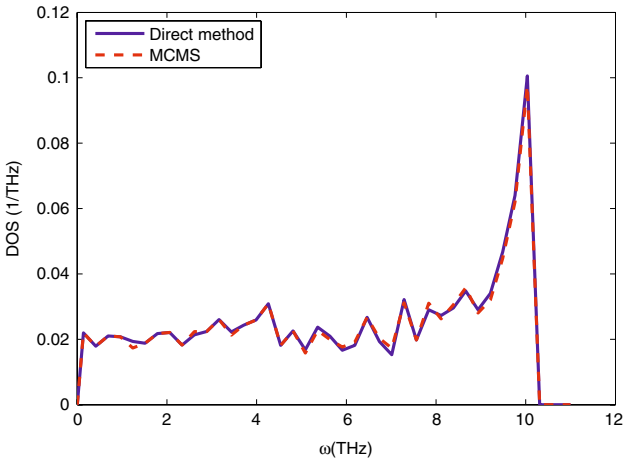

Fig. 9 PDOS of the "L"-shaped composite atom sheet

Table 4 Computational cost comparison of the MCMS discretization schemes

	Direct approach	2 levels with 16 (21 × 21) atom substructures	2 levels with 64 (11 × 11) atom substructures	4 levels with 4 equal-size substructures per level
CPU time (s)	11,235	1,785	2,221	538

substructures in a bottom-up manner. By repeating this procedure, the PDOS of the top-level nanostructure can be obtained. The proposed approach, while retains the atomic description of the nanocomposite structure, significantly reduces the computational cost of the calculation. The proposed MCMS is applied to compute the PDOS of 1-D composite atom chains and 2-D composite atom sheets. The results obtained from the MCMS are compared to those obtained from the direct method. It is shown that for a typical system of 20,000 DOFs the proposed approach reduces the CPU time by about 30 times.

References

1. Thostenson ET, Li C, Chou TW (2005) Nanocomposites in context. Composite Sci Tech 65:491
2. Hariharan S, Gass J (2005) Superparamagnetism and magnetocaloric effect (MCE) in functional magnetic nanostructures. Rev Adv Mater Sci 10(5):398
3. Tritt TM (ed) (2000) Semiconductors and semimetals. Academic Press, London, pp 69–71
4. Katsuyama S, Kanayama Y, Ito M, Majima K, Nagai H (2000) Thermoelectric properties of $CoSb_3$ with dispersed $FeSb_2$ particles. J Appl Phys 88(6):3484
5. Yang R, Chen G (2004) Thermal conductivity modeling of periodic two-dimensional nanocomposites. Phys Rev B 69:195316
6. Sanchez C, Julian B, Belleville P, Popall M (2005) Applications of hybrid organic-inorganic nanocomposites. J Mater Chem 15(35–36):3559
7. Goyal RK, Tiwari AN, Mulik UP, Negi YS (2007) Novel high performance $A1_2O_3$ /poly(ether ether ketone) nanocomposites for electronics applications. Composite Sci Tech 67:1802
8. Tang Z, Zhao H, Li G, Aluru NR (2006) Finite-temperature quasicontinuum method for multiscale analysis of silicon nanostructures. Phys Rev B 74:064110
9. Zhao H, Tang Z, Li G, Aluru NR (2005) Quasiharmonic models for the calculation of thermodynamic properties of crystalline silicon under strain. J Appl Phys 99:064314
10. Porter LJ, Justo JF, Yip S (1997) The importance of Gruneisen parameters in developing interatomic potentials. J Appl Phys 82:5378
11. Li J, Porter L, Yip S (1998) Atomistic modeling of finite-temperature properties of crystalline beta-SiC. II. Thermal conductivity and effects of point defects. J Nuclear Mater 255:139
12. Grimvall G (1981) The electron–phonon interaction in metals. North–Holland, Amsterdam
13. Ashcroft NW, Mermin ND (1976) Solid state physics. Harcourt, New York

14. Maradudin AA, Montroll EW, Weiss GH, Ipatova IP (1971) Theory of lattice dynamics in the harmonic approximation. Academic Press, London
15. Wallace DC (1972) Thermodynamics of crystals. Wiley, London
16. Cunedioglu Y, Mugan A, Akcay H (2006) Frequency domain analysis of model order reduction techniques. Finite Elem Anal Des 42:367
17. Craig RR Jr, Bampton MCC (1968) Coupling of substructures for dynamic analysis. AIAA J 6:1313
18. Min KW, Igusa T, Achenbach JD (1992) Frequency window method for forced vibration of structures with connected substructures. J Acoust Soc Am 92(5):2726
19. Shyu WH, Ma ZD, Hulbert GM (1997) A new component mode synthesis method: quasi-static mode compensation. Finite Elem Anal Des 24:271
20. Shyu WH, Gu J, Hulbert GM, Ma ZD (2000) On the use of multiple quasi-static mode compensation sets for component mode synthesis of complex structures. Finite Elem Anal Des 35:119
21. Markovic D, Park KC, Ibrahimbegovic A (2007) Reduction of substructural interface degrees of freedom in flexibility-based component mode synthesis. Int J Numer Meth Eng 70:163
22. Girifalco LA, Lad RA (1956) Energy of cohesion, compressibility, and the potential energy functions of the graphite system. J Chem Phys 25:693
23. Morse PM (1929) Diatomic molecules according to the wave mechanics. II. Vibrational levels. Phys Rev 34:57
24. Tersoff J (1988) Empirical interatomic potential for silicon with improved elastic properties. Phys Rev B 38:9902
25. Brenner DW (1990) Empirical potential for hydrocarbons for use in simulating the chemical vapor deposition of diamond films. Phys Rev B 42:9458
26. Stillinger FH, Weber TA (1985) Computer simulation of local order in condensed phases of silicon. Phys Rev B 31:5262
27. Tomar V, Zhou M (2006) Classical molecular-dynamics potential for the mechanical strength of nanocrystalline composite fcc Al + $\alpha - Fe_2O_3$. Phys Rev B 73:174116
28. Baskes MI (1992) Modified embedded-atom potentials for cubic materials and impurities. Phys Rev B 46:2727
29. Besson R, Morillo J (1997) Development of a semiempirical n-body noncentral potential for Fe–Al alloys. Phys Rev B 55:193